RSC Advances

PAPER

View Article Online
View Journal | View Issue

Check for updates

Cite this: *RSC Adv.*, 2025, **15**, 25742

Trevesia palmata-derived terpenoid-rich silver nanoparticles induce apoptosis and upregulate p21/CAV1 proteins in gastric cancer cells†

Van Hung Hoang,[a] Thi Thanh Huong Le,[b] Thi Tam Khieu,[b] Thi Ngoc Thuy Le,[c] Thi Kieu Oanh Nguyen[d] and Phu Hung Nguyen *[ac]

Received 9th May 2025
Accepted 8th July 2025

DOI: 10.1039/d5ra03268g

rsc.li/rsc-advances

Cancer remains one of the most prevalent and deadly diseases, ranking among leading global causes of morbidity and mortality. This study presents the green synthesis of silver nanoparticles using *Trevesia palmata* leaf extract (Trp-AgNPs) and evaluates their anticancer efficacy. Trp-AgNPs formation was confirmed by the color transition of the solution from transparent to brown, along with a prominent UV-Vis absorption peak at 436 nm. X-ray diffraction (XRD) and Fourier-transform infrared spectroscopy (FTIR) confirmed the crystalline structure of the Trp-AgNPs and the presence of biomolecules contributing to reduction and stabilization. Transmission electron microscopy (TEM) analysis identified spherical nanoparticles with an average diameter of 17.84 ± 8.28 nm. QToF-MS analysis indicated that 26 different compounds, including 14 bioactive terpenoids, were bound to the surface of the silver nanoparticles. The anticancer properties of Terpenoid-rich Trp-AgNPs were evaluated across four cancer cell lines (MKN45, HepG2, MCF7, and A549), with MKN45 demonstrating the highest sensitivity ($IC_{50} = 0.5\ \mu g\ mL^{-1}$). Flow cytometry revealed dose-dependent apoptosis in MKN45 cells induced by Trp-AgNPs. Trp-AgNPs upregulated the transcription of Caspase 8, Caspase 3, P21, and Caveolin-1 (CAV1) genes. Significantly, the mRNA expression of P21 increased by more than five-fold, while CAV1 demonstrated an approximately eleven-fold increase, indicating their potential role in cytotoxicity. Additionally, strong binding of nanoparticle surface compounds to anti-apoptotic proteins, as shown by molecular docking, reveals how Trp-AgNPs induce apoptosis signaling in gastric cancer cells. These findings highlight the potential of Trp-AgNPs as a targeted, eco-friendly therapeutic strategy for gastric cancer.

1 Introduction

Cancer remains one of the most prevalent and lethal diseases globally, consistently ranking among the leading causes of morbidity and mortality worldwide.[1] Despite significant advances in treatment techniques and surgical tumor resection, the mortality rate associated with gastric cancer remains high, primarily due to the development of therapeutic resistance in cancer cells.[2] This reality has driven ongoing research and improvements in treatment modalities, with particular emphasis on the discovery and development of novel anticancer drugs that have fewer side effects and are derived from plant sources.[3,4] Additionally, the fabrication of bio-nanomaterials has emerged as a crucial tool, garnering significant attention due to their enhanced biocompatibility, environmental sustainability, and markedly improved biological activity.[5] Nanotechnology, notably the synthesis of silver nanoparticles (AgNPs), has recently garnered significant attention due to its applications in the medical field, including potential anticancer effects.[6] Owing to their small size, high surface area, and ability to interact with various chemical functional groups, AgNPs demonstrate distinct advantages in biological activity, thereby enhancing their cytotoxic efficacy against cancer cells. The green synthesis also known as biosynthesis of silver nanoparticles using plant extracts is regarded as a simple, cost-effective, and environmentally friendly approach.[7] There have also been comparative studies showing that green-synthesized silver nanoparticles have higher biocompatibility and fewer negative effects on embryo development compared to chemically synthesized nanoparticles.[8] Natural compounds present in plant extracts exhibit reducing properties that facilitate the conversion of silver ions into silver nanoparticles, while

---

[a] Thai Nguyen University, Tan Thinh Ward, Thai Nguyen City, Vietnam. E-mail: hungnguyenphu@tnus.edu.vn; Tel: +84 818432886

[b] Thai Nguyen University of Sciences, Tan Thinh Ward, Thai Nguyen City, Vietnam

[c] Center for Interdisciplinary Science and Education, Thai Nguyen University, Tan Thinh Ward, Thai Nguyen City, Vietnam

[d] Ha Noi University of Science and Technology (USTH), Hoang Quoc Viet, Ha Noi, Vietnam

† Electronic supplementary information (ESI) available. See DOI: https://doi.org/10.1039/d5ra03268g

concurrently capping their surfaces to stabilize the nanoparticles and enhance their biological activity.[9] Moreover, these plant-derived compounds serve as an important source for the development of therapeutic agents or health supplements against cancers, owing to their diverse biological activities such as inducing apoptosis, inhibiting angiogenesis or cell migration.[10,11] Accumulating evidence indicates that the anticancer mechanisms of AgNPs are very complex. Common mechanisms include enhancing the overproduction of ROS within cells, causing DNA strand breaks in the cell nucleus, and inducing apoptosis.[12] In addition, AgNPs have been shown to cause cell cycle arrest and interfere with various cancer signaling pathways, such as the PI3K/Akt/mTOR pathway and mitochondrial-mediated apoptosis cell death signaling pathways.[13]

Trevesia palmata (Roxb. Ex Lindl.) Vis. is recognized as an herbal species widely distributed across many Southeast Asian countries and the Himalayan region. This herb has long been utilized in traditional medicine in several Southeast Asian, Chinese and India countries to treat a variety of ailments, including arthritis, thrombosis, tissue hyperplasia, and other disorders.[14,15] The diverse chemical composition of *Trevesia palmata* contributes to its rich spectrum of biological activities. Studies have shown that this plant contains various triterpenoids, flavonoids, and phenolic acids, which exhibit anti-inflammatory, antioxidant, antibacterial, and antiproliferative effects against osteosarcoma.[16,17] However, data on the anticancer activity of this medicinal herb is generally limited. This study aims to synthesize silver nanoparticles using *Trevesia palmata* leaf extract and assess their anticancer efficacy in gastric cancer cells. By combining the benefits of green nanotechnology with the medicinal properties of *Trevesia palmata*, this study aims to develop a silver nanoparticle-based nanocomplex that is both highly effective against cancer cells and environmentally sustainable.

2 Material and methods

2.1. Preparation of *Trevesia palmata* leaf extract

The *Trevesia palmata* specimen was collected in Thai Nguyen Province, Vietnam, at coordinates N 21°32′57.6″ E 105° 46′45.30″ and identified by Dr Thi Thanh Huong Le. The voucher specimen (TNU2024.11) is deposited at the Faculty of Biotechnology, Thai Nguyen University of Sciences.

The leaves of *Trevesia palmata* were finely ground into a powder. Subsequently, five grams of this powder were weighed and added to a glass container with 100 mL of deionized water.

The mixture was agitated for 10 minutes and subsequently heated to boiling for 15 minutes. The obtained extract was filtered through Whatman filter paper (20 cm diameter) to remove the residual leaf debris, and then stored at 4 °C for subsequent experiments.

2.1.1 Green synthesis of silver nanoparticles. A 5 mM silver nitrate ($AgNO_3$) solution was prepared using deionized water. Next, 3 mL of the previously prepared *Trevesia palmata* leaf extract was added to 90 mL of the 5 mM $AgNO_3$ solution and stirred gently at 250 rpm at 60 °C. The formation of silver nanoparticles was monitored by the color change of the reaction mixture from colorless to brown, indicative of the surface plasmon resonance phenomenon. Samples were taken at time intervals of 0, 5, 10, 15, 20, 25, and 30 minutes for UV-Vis spectral analysis to track the development of the characteristic absorption peak. The solution was then centrifuged at approximately 10 000 rpm for 15 minutes to collect the nanoparticle precipitate, which was subsequently washed three times with deionized water and stored at 4 °C for further biological activity assays.[18]

2.2. Ultraviolet-visible spectroscopy

The silver nanoparticle solution was analyzed using a UV-Vis spectrophotometer (Multiscan-Sky, Thermo Fisher) over a wavelength range of 300–1000 nm to determine the surface plasmon resonance peak of the AgNPs.

2.2.1 X-ray diffraction analysis. The silver nanoparticle powder sample was obtained by drying the nanoparticle solution. XRD measurements were carried out using X-ray diffractometer (D2-Phase, Brucker, Japan), with a scanning range of 2θ from 20° to 80°. The diffraction peaks were compared against standard data (JCPDS) to ascertain the crystalline structure of silver, which is typically a face-centered cubic (FCC) arrangement.[18]

2.3. Fourier transform infrared spectroscopy

Dried silver nanoparticle samples were mixed with KBr to form pellets, and FTIR spectra were recorded in the range of 4000–400 cm^{-1} using a PerkinElmer Spectrum Two spectrometer (Spectrum Two, USA). This analysis was performed to identify the functional groups involved in the reduction and stabilization of the nanoparticles as previously described.[19]

2.4. Transmission electron microscopy (TEM) and dynamic light scattering analysis

For Transmission electron microscopy (TEM) analysis, a drop of the silver nanoparticle solution was deposited onto a carbon-coated copper grid and allowed to air dry. The morphology and size of the nanoparticles were observed using a scan electron microscope (JEOL 2100F), which operated at 80 kV, direct mag 100 K. Nanoparticle dimensions were measured and analyzed using image analysis ImageJ software.

Zeta potential and particle size distribution of the synthesized AgNPs were analysed using a dynamic light scattering (DLS) instrument (Horiba SZ-100), with a zeta potential range of −500 to +500 mV and particle size range of 0.3 nm to 10 μm.

2.5. Identification of natural compounds on the surface of silver nanoparticles

The identification of chemical components on the surface of silver nanoparticles was carried out using UPLC-QToF mass spectrometry (Waters Corporation, USA).[20] After synthesis, the nanoparticles were washed repeatedly with deionized H_2O, mixed thoroughly by pipetting, followed by centrifugation at 15 000 rpm, and the supernatant was removed. This process was repeated three times to remove unbound compounds from the nanoparticles. Subsequently, the sample was prepared by dissolving 0.1 mg of nanoparticles in 0.5 mL of methanol, filtered through a 0.22 μm membrane, and 1 μL was injected for chromatographic separation using a BEH C18 column. Mass spectra were acquired in both positive and negative electrospray ionization modes under optimized conditions. Data were acquired in full scan mode (m/z 50–1100), and fragmentation data were obtained using low and high collision energy modes. Spectral data were processed using UNIFI software, and peak annotation was performed based on comparing fragmentation patterns against the Waters Traditional Medicine Library (Waters Corporation, USA).

2.6. Cell culture and MTT assay

Cancer cells (Gastric cancer (MKN45), liver cancer (HepG2), breast cancer (MCF7), and lung cancer (A549) from Bordeaux Institute of Oncology, France) were seeded in 96-well plates at a density of approximately 8×10^3 cells per well and incubated for 24 hours to ensure adherence. The medium was then replaced with fresh medium containing various concentrations of AgNPs (0.2, 0.5, 1.0, 1.5, and 2.0 μg mL^{-1}), while the control group received no treatment. After an additional 48 hours of incubation, the medium was removed and 100 μL of new culture medium containing 0.5 mg per mL MTT was added. The plates were incubated for 4 h at 37 °C. The MTT solution was subsequently removed, and 100 μL of DMSO was added to dissolve the formazan crystals. Optical density (OD) was measured at 570 nm using a Multiskan Sky microplate reader (Thermo Fisher, Massachusetts, USA) as previously described.[11]

2.7. Apoptosis analysis by flow cytometry

Apoptosis was evaluated following the protocol of Carlo Riccardi and Ildo Nicoletti.[21] MKN45 cells were seeded and treated with various concentrations of Trp-AgNPs (0.5, 1.0, and 1.5 μg mL^{-1}) for 48 hours, and then fixed in 70% ethanol at 4 °C for 2 h. The fixed cells were incubated with a 20 μg per mL propidium iodide (PI) solution for 1 h. Flow cytometry was subsequently performed using a 488-nm laser, with twenty thousand events acquired per sample and analyzed using C6 Plus Analysis Software (BD Bioscience, USA) as previously reported.[22]

2.8. RNA isolation and real-time PCR analysis

MKN45 cells were treated with Trp-AgNPs at the IC$_{50}$ concentration (0.5 μg mL^{-1}) for 24 hours, then harvested for total RNA extraction using a TRIzol@ Reagent (Thermo Fisher, USA). RNA concentration and purity were determined using a spectrophotometer (NanoDrop). Complementary DNA (cDNA) was synthesized from the extracted RNA using reverse transcriptase. Real-time PCR using the BIOFACT 2x SYBR Green IOnestep Master Mix qRT-PCR (BIOFACT, Korea) were performed according to the manufacturer's instructions with specific primers for target genes, including Caspase 3, Caspase 8, Caspase 9, Bcl-2, P21, CAV1 and a HPRT-1 housekeeping gene (Table S1†). The reactions were run on a the qTower3 system (Analytik Jena, Jena, Germany) and analyzed using the $2^{-\Delta\Delta C_t}$ method to compare gene expression levels between treated and control samples as previously described.[23]

2.9. Immunofluorescence analysis

Cells were cultured on coverslips in 24-well plates until reaching an appropriate density and then treated with Trp-AgNPs at the IC$_{50}$ concentration for 24 hours. The cells were fixed with 4% paraformaldehyde for 30 minutes, permeabilized with 0.05% Triton X-100 for 5 minutes, and blocked with 3% BSA for 30 minutes. Subsequently, the cells were incubated with primary antibodies against P21 or CAV-1 (all from Abcam, Cambridge, USA) at room temperature for 30 minutes, followed by PBS washes. The cells were then incubated with fluorophore-conjugated secondary antibodies. After counterstaining the nuclei with DAPI and washing twice with PBS, the samples were observed and imaged using a Nikon Ti2 fluorescence microscope, and images were analyzed with specialized software (NIS-Elements 5.0, Nikon, Japan) as previously reported.[24]

2.10. Molecular docking

Preparation of ligand and protein: The 26 compounds (Table 2) were obtained from the PubChem database in SDF format or redrawn using ChemDraw 23.1.1. Ligand structures were processed using LigPrep at pH 7 ± 2, with the OPLS4 force field applied to generate all relevant tautomers and stereoisomers in their lowest energy 3D conformations. The crystal structures of Bcl-2 (PDB ID: 6GL8), Bcl-XL (3ZK6), Bcl-W (2Y6W), Mcl-1 (4OQ6), XIAP (5OQW), Survivin (3UIH), AKT (4GV1), and mTOR (4JT5), were retrieved from the Protein Data Bank and prepared using the Protein Preparation Wizard. Binding sites were defined based on co-crystallized ligands present in each PDB structure. The grid box parameters for each target protein are presented in Table 1.

Table 1 Docking grid coordinates and box dimensions for target proteins

Protein	Grid center (x, y, z, Å)	Inner box (Å)	Outer box (Å)
Bcl-2	(16.247, 2.004, 16.359)	10 × 10 × 10	26.719 × 26.719 × 26.719
Bcl-XL	(20.404, 50.089, 1.617)	10 × 10 × 10	34.781 × 34.781 × 34.781
Bcl-W	(−18.170, 5.000, −1.000)	35 × 35 × 35	26.622 × 26.622 × 26.622
Mcl-1	(13.516, 10.616, 10.264)	10 × 10 × 10	24.451 × 24.451 × 24.451
XIAP	(22.486, −1.783, −20.875)	10 × 10 × 10	25.179 × 25.179 × 25.179
Survivin	(−31.822, 29.266, 65.689)	10 × 10 × 10	25.896 × 25.896 × 25.896
AKT	(−19.930, 4.348, 11.200)	10 × 10 × 10	24.816 × 24.816 × 24.816
mTOR	(51.398, −0.188, −49.016)	10 × 10 × 10	24.523 × 24.523 × 24.523

Molecular docking and binding affinity evaluation: docking reliability was assessed by redocking the cocrystallized ligands into their original binding sites. The protocol was considered valid when the root-mean-square deviation (RMSD) between the redocked and experimental poses was less than 2.0 Å. All 26 compounds were subsequently docked into the prepared protein structures using the Glide Extra Precision (XP) algorithm. Binding free energies were estimated using the MM-GBSA (Molecular Mechanics/Generalized Born Surface Area) method, employing the VSGB implicit solvation model and the OPLS4 force field.

2.11. Statistical analysis

Statistical comparisons were performed using the Mann–Whitney *U* Test, with analysis conducted using GraphPad Prism 10.0 (GraphPad Software, Inc.).

3 Results and discussion

3.1. Green synthesis of silver nanoparticles using *Trevesia palmata* extract

The silver nanoparticle synthesis (Fig. 1) is confirmed by the change in color from transparent to brown when the *Trevesia palmata* leaf extract is added to the $AgNO_3$ solution, reflecting the characteristic surface plasmon resonance phenomenon of silver nanoparticles (Fig. 1B). UV-Vis spectral analysis revealed the presence of a characteristic absorption peak at 436 nm, which corresponds to the surface plasmon resonance of silver nanoparticles (Fig. 1C). The progressive increase in absorption peak intensity over time indicates a robust reduction of Ag^+ ions into nanoparticles, leading to a progressive increase in the concentration of generated silver nanoparticles. Subsequently, Trp-AgNPs were characterized using SEM and TEM, XRD, and FTIR spectroscopy.

The green synthesis of AgNPs using plant extracts is regarded as an eco-friendly alternative to conventional chemical methods, which are inherently associated with the risk of environmental pollution.[25] This study employed the boiling extraction method, which enables a shortened synthesis time of only 10–20 minutes while avoiding the residual presence of undesirable compounds commonly associated with solvent-based methods such as ethanol, methanol, or hexane. The *Trevesia palmata* Roxb. extract was employed as a reducing agent to convert silver ions from $AgNO_3$ salt into silver nanoparticles. The color change of the silver salt solution from colorless to yellow and then to dark brown, along with the characteristic absorption peak observed at 436 nm in the UV-Vis spectrum, confirmed the formation of AgNPs *via* the surface plasmon resonance phenomenon. These observations are consistent with previously published studies on plant-mediated synthesis of AgNPs, in which the absorption peak is typically recorded in the range of 400–450 nm.[26]

3.2. Characteristics of the X-ray diffraction spectrum and Fourier transform infrared spectroscopy of Trp-AgNPs

XRD analysis (Fig. 2A) revealed diffraction peaks at 2θ angles of 27.74°, 32.26°, 38.18°, 43.77°, 64.02°, and 77.37°, with the most intense peak at $2\theta = 43.77°$ corresponding to the (200) crystal plane of silver. This indicates that the Trp-AgNPs display the characteristic crystalline structure of silver, featuring a face-centered cubic arrangement. These findings also confirm the

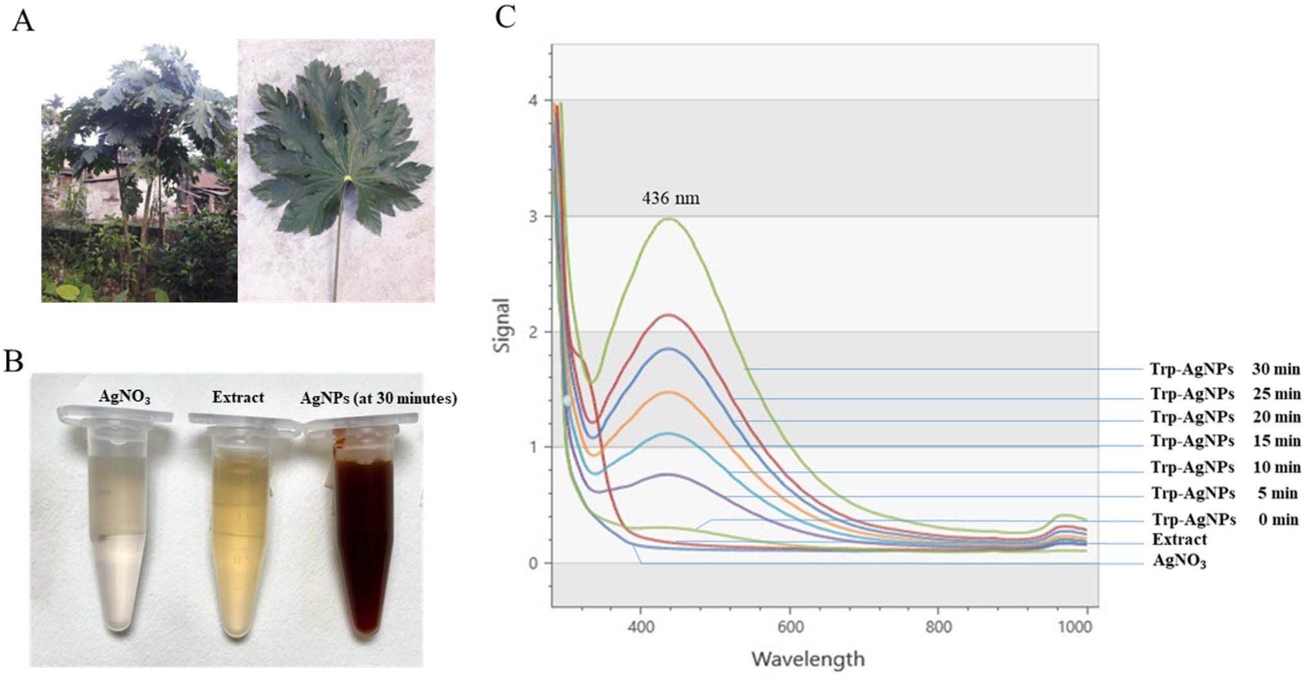

Fig. 1 Synthesis of silver nanoparticles using *Trevesia palmata* leaf extract. Plant and leaf sample of *Trevesia palmata* (A), color of the synthesized nanoparticle solution (B), and UV-Vis absorption spectrum of silver nanoparticle samples over time (C).

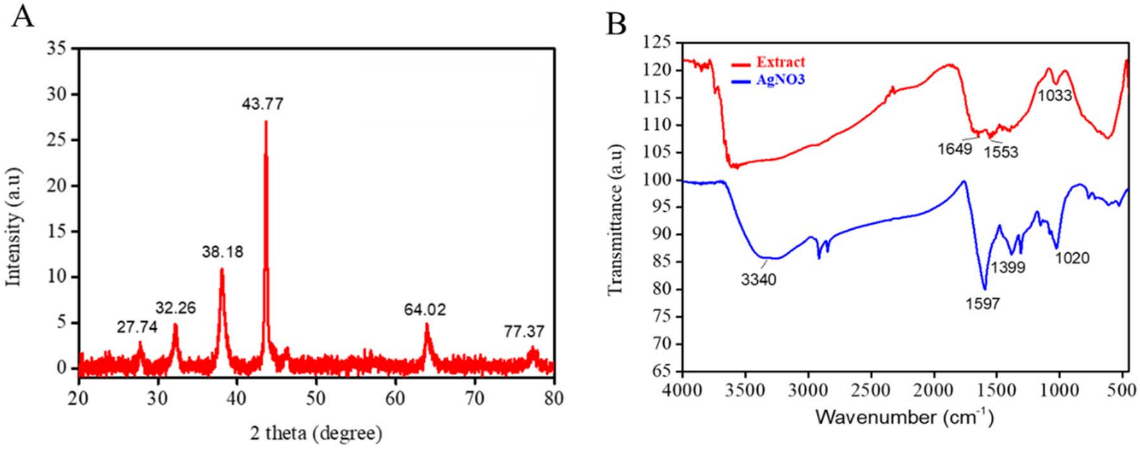

Fig. 2 X-ray diffraction analysis spectrum (A) and Fourier-transform infrared spectroscopy spectrum (B) of the synthesized silver nanoparticles.

successful synthesis of silver nanoparticles. The FTIR spectrum (Fig. 2B) revealed that functional groups are bound to the silver nanoparticles, contributing to their stabilization. Typical absorption peaks were identified at 3410 cm^{-1} (O–H or N–H stretching), 1649 cm^{-1} (C═O stretching of carbonyl or amide I), 1553 cm^{-1} (bending or amide II), 1399 cm^{-1} (C–H bending), and 1020–1033 cm^{-1} (C–O or C–N stretching). These spectral data underscore the interaction between the compounds present in the *Trevesia palmata* extract and the nanoparticle surface, serving as both reducing and stabilizing agents. Accordingly, the combined XRD and FTIR data presented in Fig. 2 confirm the successful biosynthesis of AgNPs with the incorporation of biomolecules from *Trevesia palmata*, potentially enhancing both their stability and biological activity.

Trp-AgNPs synthesized in this study exhibit a face-centered cubic structure as determined by XRD analysis. The FTIR spectrum reveals the presence of functional groups such as O–H, C═O, N–H, and C–O, which are attributed to the bioactive compounds present in the *Trevesia palmata* extract. These findings are consistent with previous reports on AgNP synthesis using *Syngonium podophyllum*,[27] and *Olea europaea* extract.[28] The integration of UV-Vis, TEM, XRD, and FTIR data underscores the successful biosynthesis of Trp-AgNPs.

3.3. Transmission electron microscopy images of Trp-AgNPs

TEM analysis (Fig. 3) reveals that the synthesized Trp-AgNPs exhibit a spherical morphology, with sizes ranging from approximately 10 nm to over 40 nm; most particles are within the 15–25 nm range, with an average diameter of 17.84 ± 8.28 nm. The nanoparticles display uniform dispersion without significant aggregation. Some larger particles observed may result from localized variations in the concentration of the reducing agent during the early stages of synthesis. These findings further support the successful synthesis of Trp-AgNPs.

The formation of uniformly spherical nanoparticles, as observed through TEM imaging, has confirmed the efficacy of *Trevesia palmata* extract in serving as both a reducing agent and a structural stabilizer, a phenomenon also reported in other studies employing plant extracts for the synthesis of silver nanoparticles.[29,30] The size of the nanoparticles is closely related to their biological activity; the smaller the size, the larger the surface area, creating more opportunities for binding with various compounds in the extract and enhancing effective cellular penetration.[31,32] With an average measured size of 17.84 ± 8.28 nm, the Trp-AgNPs are relatively small, consistent with previous reports on silver nanoparticle synthesis using plant extracts, such as those derived from *Artemisia turcomanica*[33] and *Pistacia atlantica*,[34] which reported diameters ranging from 20 to 30 nm and demonstrated activity against AGS and KANTO III gastric cancer cells. However, the size of Trp-AgNPs is smaller than that of nanoparticles synthesized from *Teucrium polium* extract, which exhibit diameters ranging from 70 to 100 nm and activity against the MKN45 gastric cancer cell line,[35] yet larger than that of silver nanoparticles synthesized from *Ardisia gigantifolia* extract, which have an average diameter of 6 nm and show activity against both AGS and MKN45 gastric cancer cell lines.[36]

3.4. Dynamic light scattering and zeta potential of Trp-AgNPs

The zeta potential measurement was performed to evaluate the colloidal stability of AgNPs. It is wel established that the absolute zeta potential value of nanoparticles greater than ± 30 mV exhibits sufficient electrostatic repulsion to prevent aggregation, thereby enhancing their colloidal stability. The synthesized AgNPs displayed a zeta potential of −58.3 mV (Fig. 4), indicating strong repulsive forces among particles and high colloidal stability.

This value was notably more negative than those reported for AgNPs synthesized using *Terminalia bellirica* (−9.24 mV)[37] and *Manilkara zapota* (−27.5 mV) extracts,[38] suggesting that the phytochemical constituents in the plant extract contributed more effectively to particle stabilization through capping. While the mean average size of AgNPs was found to be 115 nm with a polydispersity index (PDI) of 0.232, indicating moderate size distribution.

The size measured by DLS includes the nanoparticle core and surrounding solution layer, which explains its larger size

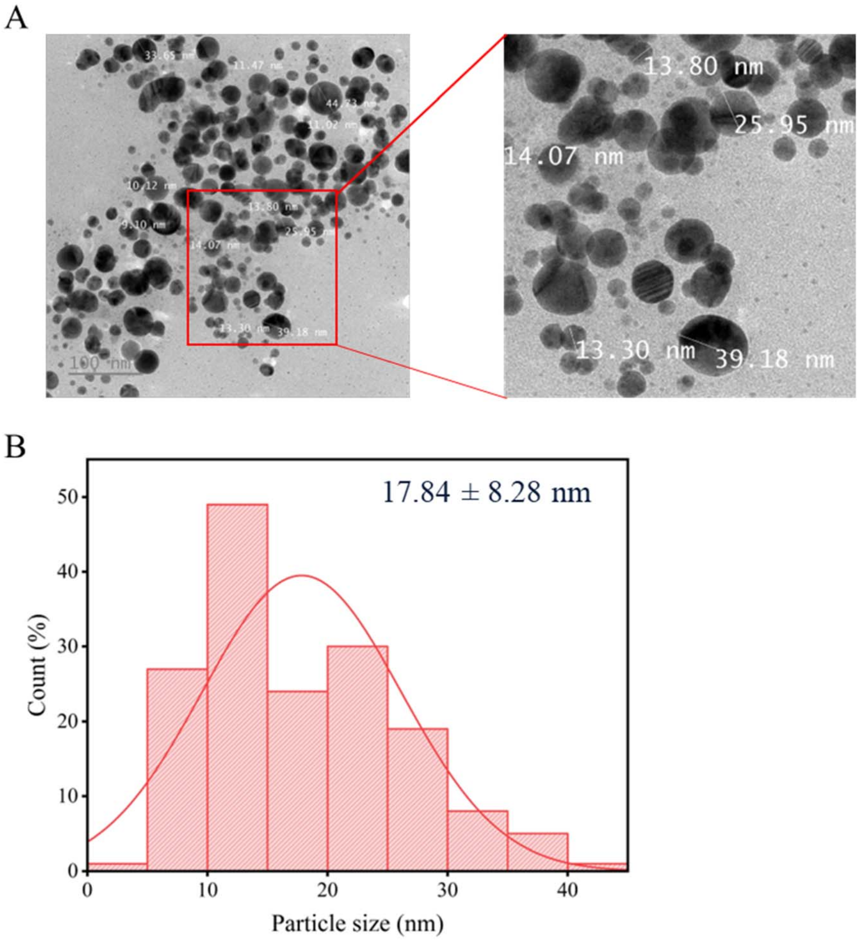

Fig. 3 Morphology captured under transmission electron microscope (A) and particle size distribution of silver nanoparticles (B).

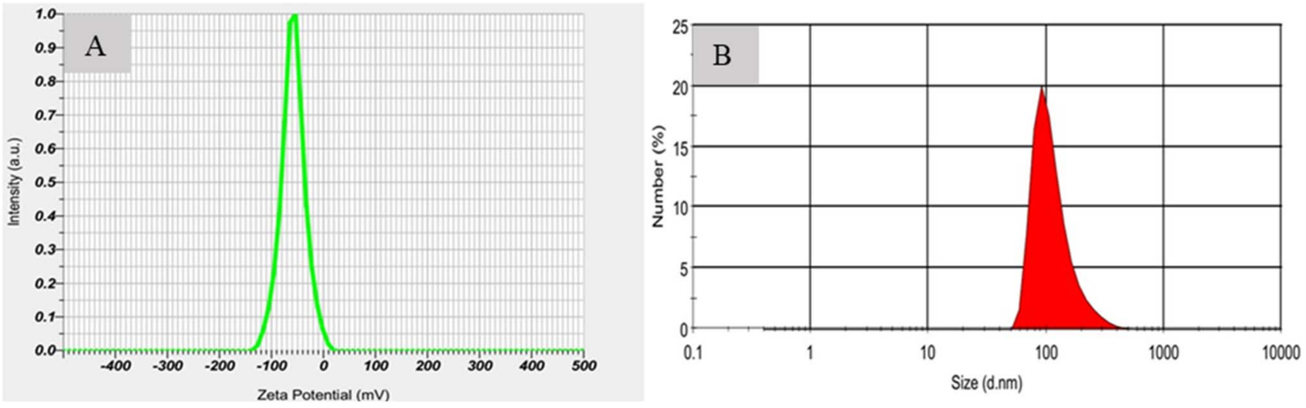

Fig. 4 Zeta potential (A) and size distribution (B) of Trp-AgNPs.

compared to TEM observations. Our findings are consistent with previous reports showing that the particle size measured by DLS is larger than that measured by TEM for green-synthesized silver nanoparticles using plant extracts from onion, tomato, and *Acacia catechu*.[39] A similar observation was reported for silver nanoparticles synthesized using *Aloe vera* extract, where the DLS-measured hydrodynamic diameter (82 nm) was significantly larger than the TEM-determined core size (5–10 nm).[40] This indicates that the solvation layer and, in particular, the plant extract play a crucial role in forming a protective shell around the silver nanoparticles, increasing the diameter many times over its core size. This shell not only supports stability but also actively participates in the biological activity of the Trp-AgNPs.

3.5. The synthesized silver nanoparticles are bound to terpenoid compounds

FTIR spectroscopic analysis (Fig. 2B) allowed for the prediction of functional groups present on the surface of the synthesized silver nanoparticles, though it could not identify specific compounds. Therefore, UPLC-QToF-MS was employed to characterize the precise chemical constituents on the surface of the tryptophan-silver nanoparticles (Trp-AgNPs). Structural elucidation of metabolites was accomplished through high-resolution mass spectrometry, with compound identification achieved by cross-referencing experimental MS/MS spectra (acquired at varying collision energies) against a comprehensive traditional medicine database. For data refinement, only peaks exceeding an intensity of 15 000 counts with mass accuracy within 5 ppm were considered. The resulting separation profiles, captured in both ionization polarities, are illustrated in Fig. 5.

Table 2 presents the compounds identified from peaks meeting the optimization criteria. A total of twenty-six different compounds were identified on the surface of Trp-AgNPs, belonging to the classes of Alkaloids, Polyphenols, Terpenoids, Flavonoids, Lignans, and other compounds. A total of 13 compounds belonged to the Terpenoid group, comprising mostly triterpenoids (10 compounds: **1**, **2**, **5**, **7**, **8**, **10**, **11**, **14**, **21**, **22**), two tetraterpenoids (compounds **15**, **17**), and two diterpenoids (compounds: **4** and **24**). Most compounds contained O–H, C–O, and C═O bonds, a few of which contained N–H bonds (compounds **16**, **19**, **20**, and **25**), reflecting consistency with the FTIR analysis results (Fig. 2B). To provide evidence for the role of natural compounds present in the extract of biological samples in the reduction of Ag^+ ions to silver nanoparticles (Ag^0) during green synthesis reactions, FTIR spectroscopy is commonly used to identify the presence of characteristic functional groups of organic compounds, such as C═O, C–O, N–H, or O–H. However, this method does not reveal which specific compounds these functional groups belong to, and this is a limitation when evaluating the contribution of natural compounds to the formation and properties of silver nanoparticles. To predict which compounds in the extract might participate in the silver ion reduction process, some studies have performed chemical composition analysis of the crude extract beforehand using highly sensitive spectroscopic methods such as UPLC-QToF-MS,[41] Gas Chromatography-Mass Spectrometry,[42] or Liquid Chromatography with Diode Array Detection and Mass Spectrometry.[43] Nevertheless, these approaches still do not allow for the conclusive confirmation of specific compounds attached to the synthesized nanoparticles. In this study, to more precisely determine which compounds participated in the reduction process and are linked to the nanoparticles after formation, we have for the first time performed direct chemical analysis of the Trp-AgNPs sample after synthesis. Repeated washing with deionized water combined with centrifugation was performed to remove unbound compounds from the Trp-AgNPs, ensuring that only the compounds bound to Trp-AgNPs were retained and detected in the analysis results. This approach allowed us to demonstrate the presence of 26 different compounds existing on the surface of Trp-AgNPs. These compounds likely exhibit strong reducing properties, having facilitated the reduction. Notably, the terpenoid class accounted for over 50% of the identified compounds. The presence of terpenoid compounds, particularly triterpenoids and tetraterpenoids, on the surface of the silver nanoparticles, which are classes of compounds known for their potent biological activities,[44] serves as significant evidence suggesting the potential anticancer activity of the Trp-AgNPs complex.

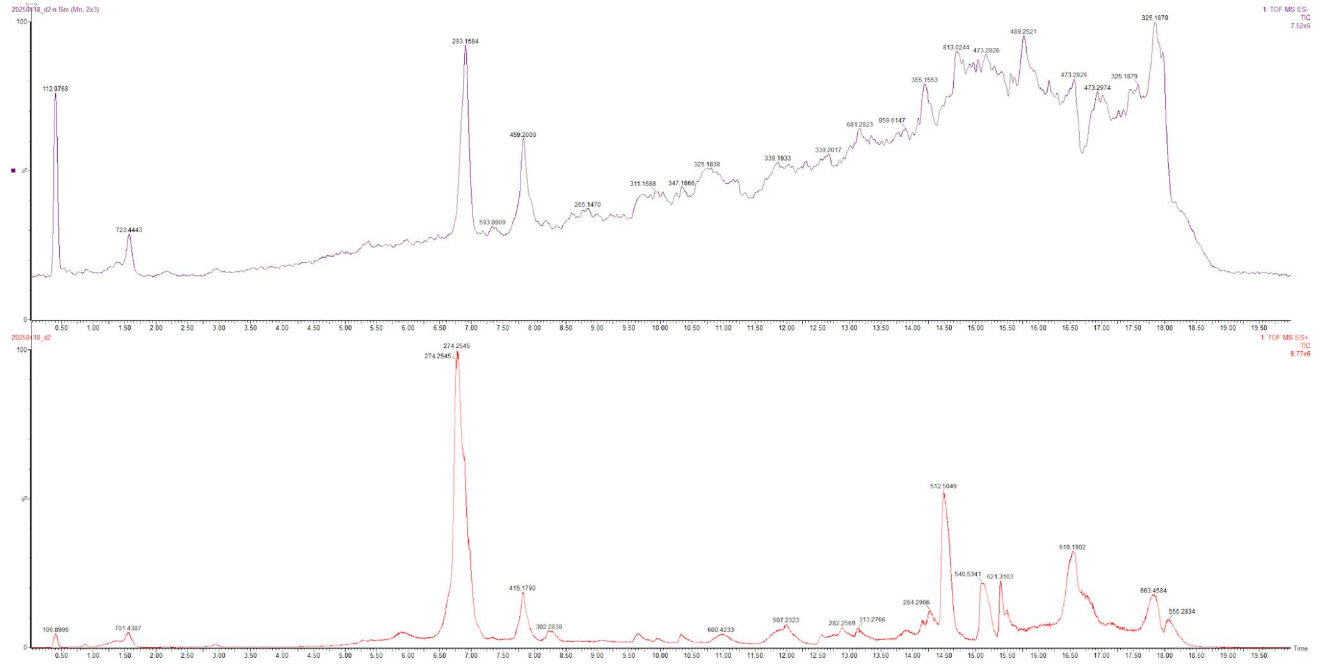

Fig. 5 UPLC-QToF-MS chromatographic profiles of Trp-AgNPs under negative (upper) and ESI positive (under) modes.

Table 2 Natural compounds identified on the surface of Trp-AgNPs[a]

No.	Component name	Formula	Observed mass (Da)	Observed RT (min)	Category	OH	C–O	C=O	N–H
1	(24*S*)-5α,8α-Epidioxy-ergost-6-en-3β-ol	$C_{28}H_{46}O_3$	430.3439	14.1473	Epidioxy sterol	✓	✓	✗	✗
2	25-*O*-Acetylcimigenol-3-*O*-β-D-xylopyranoside (23*R*,24*S*)	$C_{37}H_{58}O_{10}$	662.4029	11.8273	Saponin triterpenoid	✓	✓	✓	✗
3	6-Octadecenoic acid	$C_{18}H_{34}O_2$	282.2568	12.8964	Fatty acids	✓	✓	✓	✗
4	7-*O*-Methyl luteolin-6-C-β-D-glucoside	$C_{22}H_{22}O_{11}$	464.1335	7.94647	Flavonoid C-glycoside	✓	✓	✓	✗
5	Andrograpanin	$C_{20}H_{30}O_3$	318.2197	6.8959	Diterpenoid	✓	✓	✓	✗
6	Bistortaside	$C_{22}H_{24}O_{14}$	512.1154	14.5248	Saponin triterpenoid	✓	✓	✓	✗
7	Cimifoetiside VI	$C_{38}H_{60}O_{11}$	692.4105	10.8842	Saponin triterpenoid	✓	✓	✓	✗
8	Deglucose chikusetsusaponin IVa	$C_{36}H_{56}O_9$	632.3952	12.8149	Saponin triterpenoid	✓	✓	ND	✗
9	Deoxycholic acid	$C_{24}H_{40}O_4$	392.2911	15.5476	Triterpenoid	✓	✓	✓	✗
10	Ganoderic acid S	$C_{30}H_{44}O_3$	452.327	14.1404	Triterpenoid	✓	✓	✓	✗
11	Gypenoside XI	$C_{47}H_{76}O_{18}$	930.5547	16.678	Saponin triterpenoid	✓	✓	✓	✗
12	Hydroxysafflor yellow A	$C_{27}H_{32}O_{16}$	612.1692	16.8529	Flavonoid	✓	✓	✓	✗
13	Isoaloeresin A	$C_{28}H_{28}O_{11}$	540.163	15.13016	Polyphenol	✓	✓	✓	✗
14	Lupenone	$C_{30}H_{48}O$	424.3697	14.1932	Triterpenoid	✗	✓	✓	✗
15	Luteoxanthin	$C_{40}H_{56}O_4$	600.4156	10.9806	Tetra-terpenoid	✓	✓	✗	✗
16	*N*-Benzoyl-phenylalanine-2-benzoylamino-3-phenylpropyl ester	$C_{32}H_{30}N_2O_4$	506.2214	12.0122	Peptidomimetic esters	✗	✓	✓	✓
17	Rubixanthin	$C_{40}H_{56}O$	552.4317	16.6688	Tetra-terpenoid	✓	✓	✗	✗
18	Sanggenon A	$C_{25}H_{24}O_7$	436.1527	7.82522	Prenylated flavonoid	✓	✓	✓	✗
19	Sarmentosin	$C_{11}H_{17}NO_7$	276.1572	9.95949	Alkaloid	✓	✓	✗	✓
20	Segetalin B	$C_{24}H_{32}N_6O_5$	484.2435	12.0101	Chalcone glycoside	✓	✓	✓	✓
21	Siraitic acid C	$C_{28}H_{40}O_4$	440.2931	16.4074	Triterpenoid glycoside	✓	✓	✓	✗
22	Δ7-Stigmasterol	$C_{29}H_{46}O$	410.3541	14.6294	Phytosterol	✓	✓	✗	✗
23	(−)-Acuminatin	$C_{21}H_{24}O_4$	340.1706	6.9156	Neolignan	✓	✓	✓	✗
24	6-Gingerol	$C_{17}H_{26}O_4$	294.1854	7.81218	Phenolic ketone	✓	✓	✓	✗
25	Corynoxine B	$C_{22}H_{28}N_2O_4$	384.2026	15.5896	Oxindole alkaloid	✓	✓	✓	✓
26	Pregna-4,16-diene-3, 12,20-trione	$C_{21}H_{26}O_3$	326.1887	10.7139	Cortico-steroid	✗	✓	✓	✗

[a] ND = not determined, ✓ = Yes, ✗ = No.

3.6. Trp-AgNPs inhibit cancer cell proliferation

The cytotoxic potential of Trp-AgNPs was evaluated on MKN45, HepG2, MCF7, and A549 cell lines. Fig. 6 illustrates the effects of silver nanoparticles on the morphology and proliferation of cancer cells following a 48 hours treatment with concentrations ranging from 0.2 to 2.0 μg mL^{-1}. No morphological changes

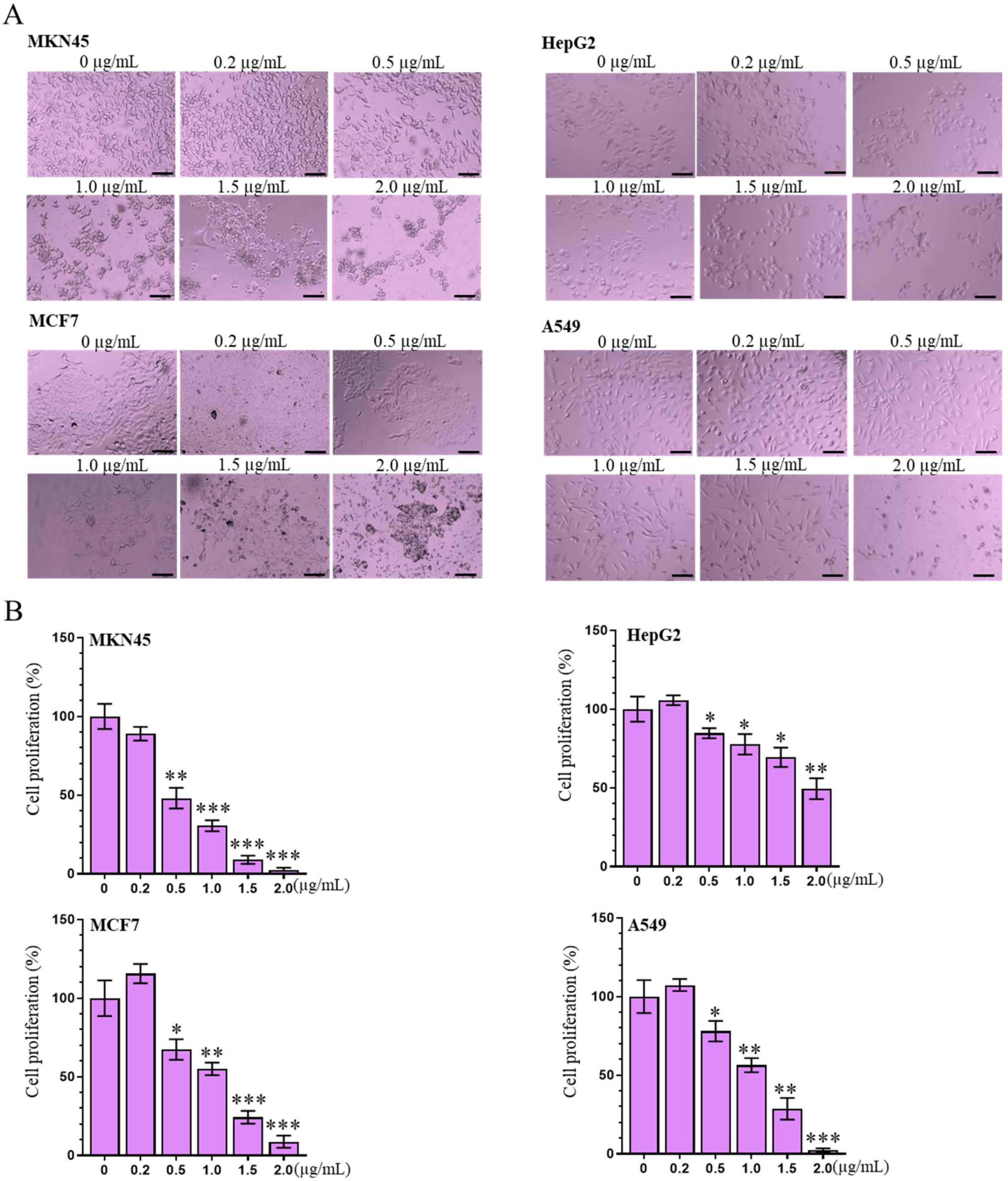

Fig. 6 The effect of silver nanoparticles on the morphology and growth of MKN45, HepG2, MCF7, and A549 cell lines. The cell lines were treated with silver nanoparticles at concentrations ranging from 0.2 to 2.0 μg mL^{-1} for 48 hours. Morphological changes were observed under an inverted microscope (A). Cell proliferation was determined by the MTT assay (B). Mann–Whitney test ($n = 4$), $*p < 0.05$, $**p < 0.01$, and $*p < 0.001$ compared to the control.

were observed in the control cells, which exhibited typical proliferation, whereas cells treated with Trp-AgNPs displayed significant morphological alterations, including the appearance of numerous small cells or dead cells detaching from the culture surface at higher concentrations. An appreciable decrease in cell proliferation was noted with escalating concentrations of Trp-AgNPs, a pattern particularly pronounced in the MKN45, MCF7, and A549 cell lines. MTT assay results confirmed a dose-dependent decrease in cell viability, with IC_{50} values of 0.5 $\mu g\ mL^{-1}$ for MKN45, 1.1 $\mu g\ mL^{-1}$ for MCF7, 1.2 $\mu g\ mL^{-1}$ for A549, and >2 $\mu g\ mL^{-1}$ for HepG2. The observed morphological changes correlated with reduced cell proliferation, indicating that the cytotoxic effects were directly induced by Trp-AgNPs. These findings suggest that Trp-AgNPs have the potential to inhibit the growth of all four cancer cell lines, with MKN45 gastric cancer cells exhibiting the highest sensitivity to the treatment.

The anti-cancer potential of Trp-AgNPs was evaluated using multiple cancer cell lines, including MKN45, HepG2, MCF7, and A549. The results demonstrated a dose-dependent reduction in cell viability, with MKN45 cells exhibiting the highest sensitivity ($IC_{50} = 0.5\ \mu g\ mL^{-1}$). The differential cytotoxicity observed among cancer cell lines may be attributed to variations in cellular uptake, as well as differences in the extent and mechanisms by which the nanoparticles affect intracellular molecular signaling pathways. This disparity has also been reported in studies evaluating the impact of green-synthesized silver nanoparticles on cancer cell lines such as HepG2, MCF7, A549, and MDA-MB-231,[45] or SW620 and SW480.[46] The IC_{50} value of 0.5 $\mu g\ mL^{-1}$ for Trp-AgNPs against MKN45 may indicate that the synthesized nanoparticles exhibit strong inhibitory activity against cancer cell proliferation compared to some green synthesized silver nanoparticles recently reported on this cell line.[47]

3.7. Trp-AgNPs induce apoptosis in MKN45 gastric cancer cells

Based on the evaluation of cytotoxicity in Fig. 5, the MKN45 cell line was found to be the most sensitive to Trp-AgNPs and was therefore selected for further apoptosis analysis and the examination of related gene expression. The nuclear staining images with DAPI (Fig. 7A) indicated that control cells exhibited a very low proportion of cells with apoptotic nuclear morphology (red arrows). The number of cells exhibiting apoptotic nuclei significantly increased in cultures treated with Trp-AgNPs. These results reflect the impact of Trp-AgNPs on the apoptotic phenotype of MKN45 cells. Flow cytometry analysis (Fig. 7B) confirmed a dose-dependent increase in apoptosis among MKN45 cells treated with silver nanoparticles. The proportion of apoptotic cells rose from 4.1 ± 1.7% in the untreated control to 8.1 ± 2.3%, 23.5 ± 2.6%, and 32.3 ± 5.7% at concentrations of 0.5 ($p < 0.05$), 1.0, and 1.5 $\mu g\ mL^{-1}$, respectively ($p < 0.001$ *versus* control). The data suggest that Trp-AgNPs induce apoptotic cell death in MKN45 gastric cancer cells in a dose-dependent fashion.

Flow cytometry analysis showed that Trp-AgNPs induced significant apoptosis in MKN45 cells. Previous studies have also indicated that AgNPs synthesized *via Scrophularia striata*, or *Phaseolus vulgaris* pod extract can induce apoptosis in various cancer cell lines, including MKN45.[48,49] As indicated by the UPLC-QToF-MS analysis results, the presence of various compounds was observed on Trp-AgNPs, where potent bioactive terpenoid compounds were predominant. Numerous previous studies have shown that compounds such as Gypenoside XI (compound **11**) induce apoptosis in gastric cancer cells HGC-27 and SGC-7901 by inhibiting the AKT/mTOR signaling pathway.[50] Hydroxysafflor yellow A has been shown to promote the expression of Caspase-3, leading to enhanced apoptosis in HepG2 liver cancer cells.[51] Furthermore, Corynoxine (compound **25**), Deoxycholic acid (compound **9**), 6-Gingerol (compound **24**), and Chikusetsusaponin IVa (compound **8**) have all been indicated to possess apoptosis-inducing and cell cycle arrest activities in various types of cancer, such as pancreatic cancer,[52] and colorectal cancer cells.[53,54] Notably, Luteoxanthin (compounds **15**), a tetratsuerpenoid present on the rface of Trp-AgNPs, has previously been shown to reverse anthracycline resistance in MCF7 breast cancer cells. These findings further reinforce the significance of the 26 identified compounds regarding the proliferation inhibitory and apoptosis-inducing roles of Trp-AgNPs against MKN45 gastric cancer cells.

3.8. Trp-AgNPs induces the expression of apoptosis signaling-related genes

Fig. 8A shows that MKN45 cells treated with 0.5 $\mu g\ mL^{-1}$ (IC_{50} value) Trp-AgNPs for 24 hours exhibit significant alterations in the expression of apoptosis-related genes. The mRNA levels of Caspase 8, Caspase 3, P21, and CAV1 increased markedly ($p < 0.05$ and $p < 0.01$ compared to control), whereas Bcl-2 remained unchanged, and Caspase 9 was reduced ($p < 0.05$). The expression of P21 increased more than five-fold compared to the control ($p < 0.01$), while CAV1 was elevated approximately eleven-fold ($p < 0.01$), indicating involvement of these factors in the cytotoxic response. Immunofluorescence images (Fig. 8B and C) further confirmed a significant increase in the protein levels of P21 and CAV1 in Trp-AgNP-treated cells, with the percentage of P21-positive cells at 65.8 ± 5.6% (*versus* 2.6 ± 1.0% in the control, $p < 0.001$) and CAV1 positive cells at 29.7 ± 6.8% (*versus* 2.8 ± 1.5% in the control, $p < 0.001$).

In the apoptotic signaling pathway, caspase genes, Bcl-2 and Bax play a central regulatory role, with extrinsic signaling initiated by Caspase 8, while Caspase 9 regulates the intrinsic pathway and Caspase 3 executes cell degradation, resulting in apoptotic morphology.[55] The effect of Trp-AgNPs on MKN45 cells resulted in differential expression of these genes; caspase 9 was observed to be downregulated, while Caspase 8 and Caspase 3 were markedly upregulated. Enhanced Caspase 8 and Caspase 3 expression has also been identified as a key factor in inducing apoptotic morphology when treating cancer cells with AgNPs synthesized from *Moringa oleifera* leaf extract or *Fagonia indica* extract.[56,57] The anti-apoptotic role of Bcl-2, mediated by the inhibition of mitochondrial cytochrome c release that prevents caspase activation, has been thoroughly investigated.[58] A marked reduction in Bcl-2 expression was observed in cells treated with

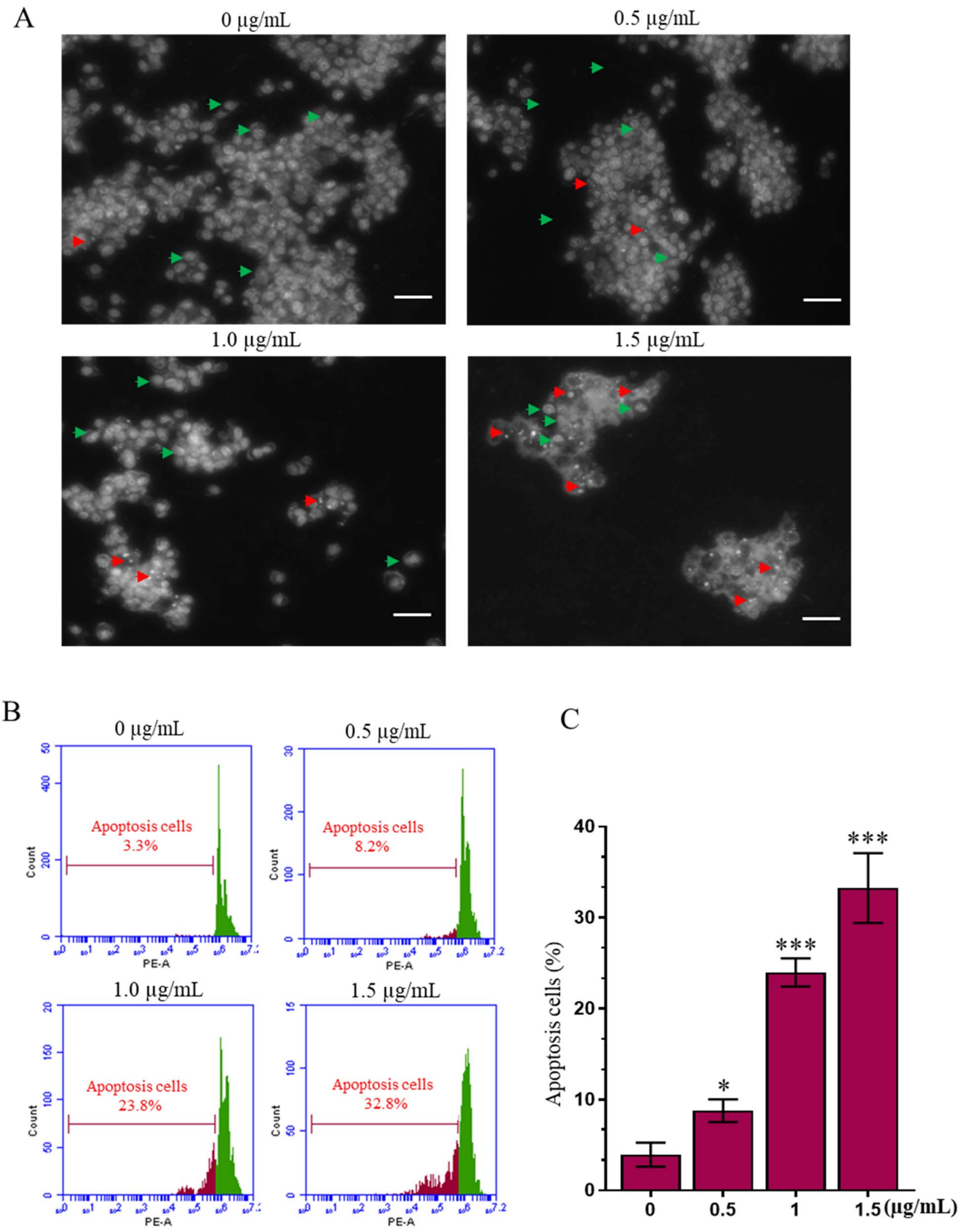

Fig. 7 The effect of silver nanoparticles on apoptosis in MKN45 cells. The cells were treated with silver nanoparticle solution at concentrations of 0.5, 1.0, and 1.5 µg mL^{-1} for 48 hours, then captured by Nikon Ti2 fluorescent microscope (A) (the green arrow indicates cells with normal nuclear morphology, while the red arrow points to cells exhibiting apoptotic nuclear features), and analyzed by flow cytometry with PI staining (B). The average percentage of apoptotic cells was calculated based on flow cytometry analysis results (C). Mann–Whitney test, $^*p < 0.05$, $^*p < 0.001$ compared to the control.

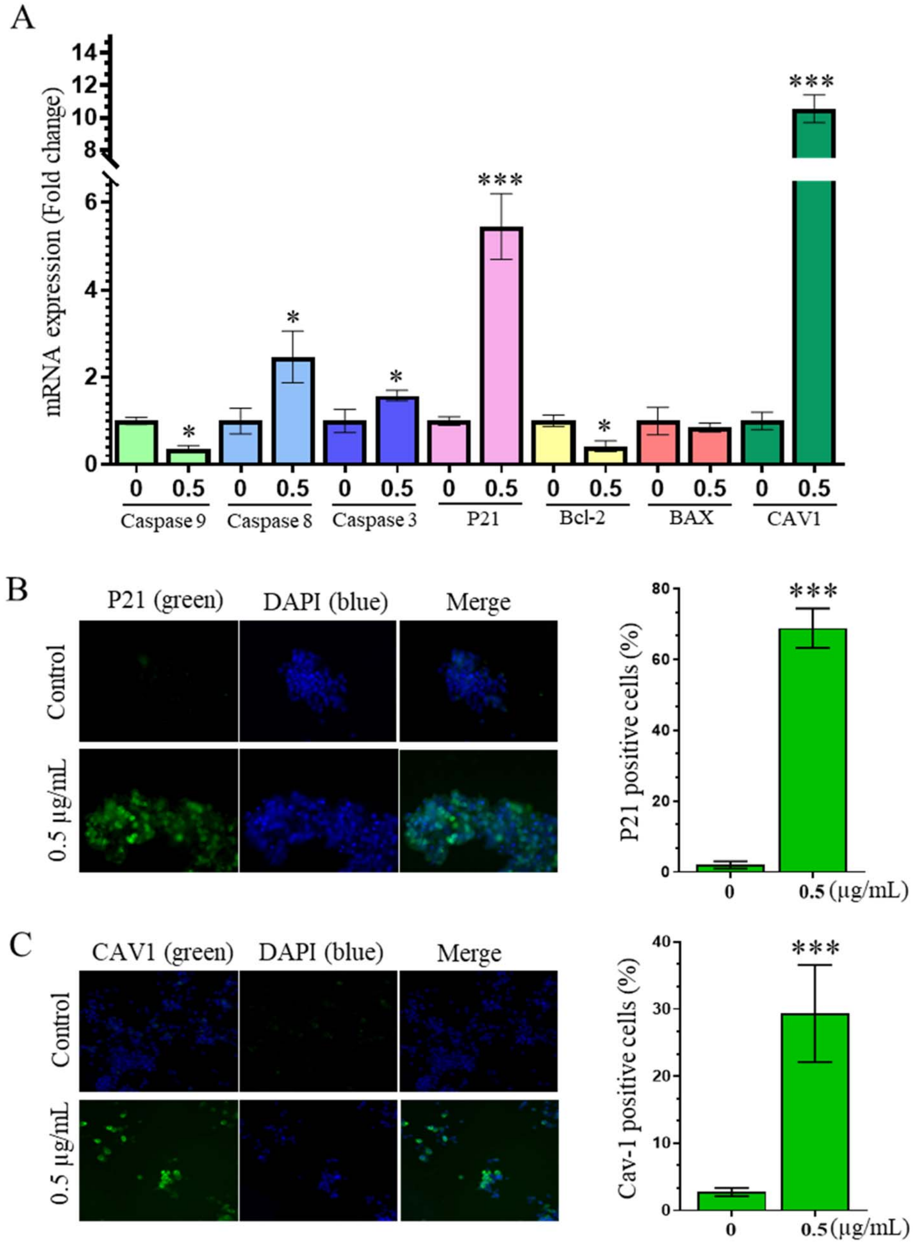

Fig. 8 Effects of Trp-AgNPs on apoptosis-related gene mRNA expression and immunofluorescent detection of P21 and CAV1 proteins in MKN45 cells. Cells were treated with Trp-AgNPs at 0.5 μg mL^{-1} for 24 hours. mRNA expresion of apoptosis realted genes was analyzed by Realtime PCR (A). P21 protein expression was deteted by immunofluorescence, (B). CAV1 protein expression was deteted by immunofluorescence (C). Mann–Whitney test, *$p < 0.05$, **$p < 0.01$, and ***$p < 0.001$ *versus* control.

Trp-AgNPs, whereas no significant alteration in Bax gene expression was detected. Notably, the data obtained from Real-time PCR analysis revealed a marked increase in gene expression, with a five-fold increase for P21 and an eleven-fold increase for CAV1 compared to controls. This significant transcriptional upregulation of P21 and CAV1 was further validated at the protein level using immunofluorescence analysis. Thus, it is evident that Trp-AgNPs altered the expression of P21 and CAV1 genes. The accumulating evidence indicates that the P21 protein plays multiple roles in cellular function, most notably in arresting the cell cycle and preventing DNA damage that can lead to carcinogenesis. However, recent *in vitro* and clinical trial evidence suggests that the excessive expression of P21 induced by treatment with therapeutic agents such as radiation, MCS-C3 (a novel analog of pyrrolopyrimidine), and oridonin has promoted apoptosis in glioblastoma and prostate cancer.[59,60] CAV1 is a multifunctional protein that plays a critical role in maintaining the structure of the cell membrane by organizing lipids and cholesterol. Additionally, it is involved in the regulation of various signaling pathways.[61] In cancer cells, deficient expression of CAV1 may promote tumor initiation, whereas increased expression is often linked to invasion and metastasis; however, in other contexts, CAV1 can induce apoptosis and inhibit cancer cell proliferation.[62] Previous reports have indicated that

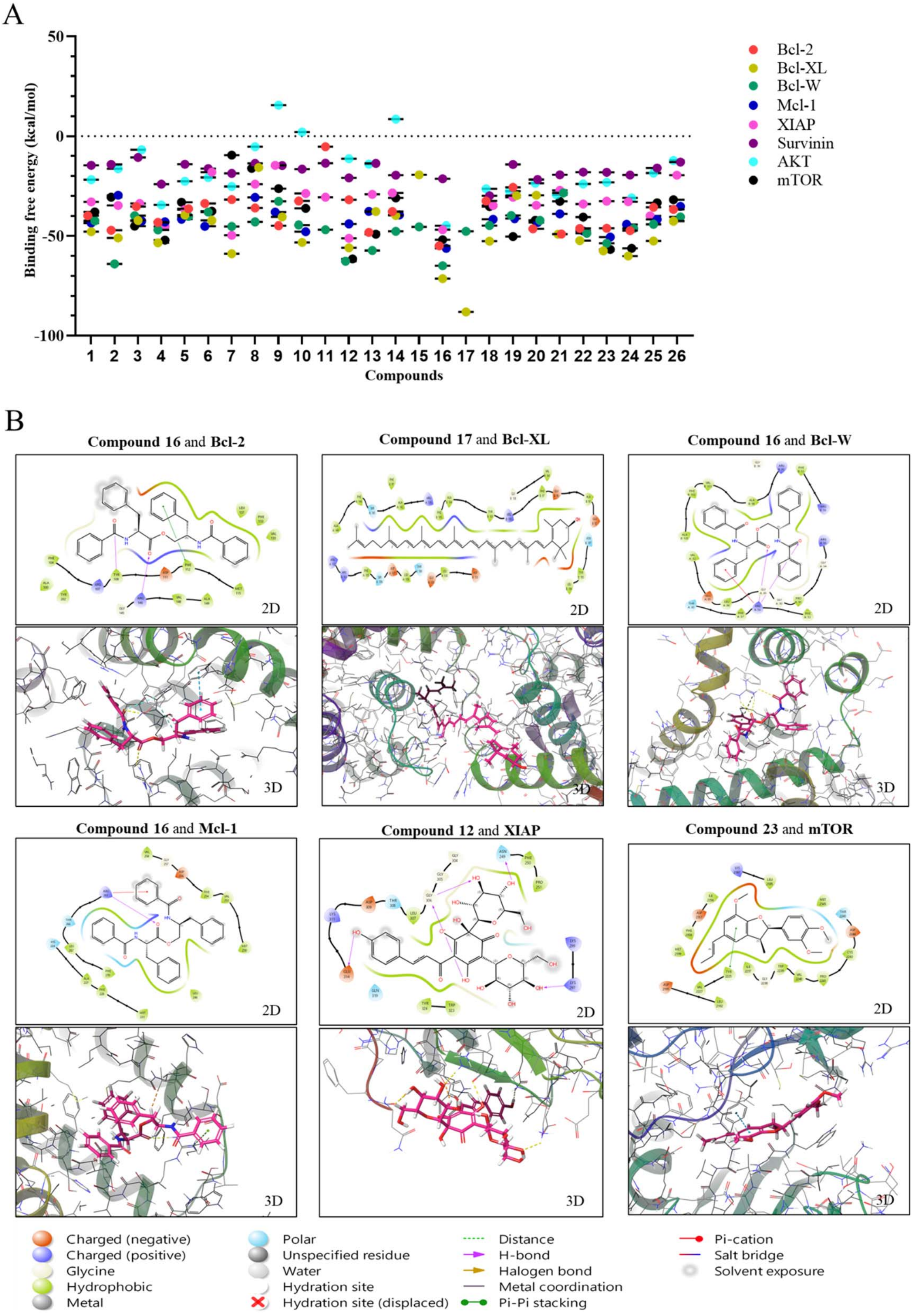

Fig. 9 Molecular docking interactions and binding poses of compounds with target proteins. (A) The graph shows the MM-GBSA binding free energy values of 26 compounds with target proteins. (B) 2D and 3D spatial interactions of compounds **16**, **17**, **12** and **23** with target proteins.

cordycepin treatment of A549 lung cancer cells induces CAV1 protein overexpression and mediates apoptosis *via* p-JNK signaling.[63] Similarly, CAV1 overexpression leads to cell cycle arrest and apoptosis induction in HL-60 cells of acute myelogenous leukemia treated with oleanolic acid.[64] In gastric cancer, clinicopathological analysis using immunohistochemical staining of tumor tissues has shown that only a small proportion of patients with primary tumors exhibit CAV1 expression,[65] whereas a separate meta-analysis indicates that high CAV1 expression is associated with a favorable prognosis, with significantly improved overall survival.[66] Thus, the overexpression of both P21 and CAV1 proteins in MKN45 cells treated with Trp-AgNPs can be considered as factors that promote apoptosis and inhibit cancer cell proliferation, and further studies using xenograft animal models will provide additional evidence supporting the therapeutic potential of Trp-AgNPs.

3.9. Compounds on the surface of silver nanoparticles strongly bind to anti-apoptotic proteins

To further clarify the effects of Trp-AgNPs on the apoptotic signaling pathway, molecular docking was performed for all 26 identified compounds (Table 2) against a panel of anti-apoptotic proteins, including Bcl-2, Bcl-W, Bcl-XL, Mcl-1, XIAP, Survivin, AKT, and mTOR. This analysis aimed to elucidate the potential of surface-bound compounds on the silver nanoparticles to inhibit the activity of these apoptosis-suppressing proteins. Based on MM-GBSA (kcal mol^{-1}) analysis (Fig. 9), several compounds exhibited the strongest binding affinities to the selected target proteins, which are key regulators of apoptosis inhibition. Specifically, Compound **16** demonstrated robust binding to Bcl-2 (-54.9 kcal mol^{-1}), Bcl-W (-64.9) and Mcl-1 (-56.2 kcal mol^{-1}), while Compound **17** revealed a potent binding affinity for Bcl-XL (-88.1 kcal mol^{-1}). Concurrently, XIAP exhibited optimal binding with compound **12** (-51.1 kcal mol^{-1}). mTOR proteins was strongly inhibited by compounds **23** and **24**, with MM-GBSA values reaching -56.7 kcal mol^{-1} and -56.2 kcal mol^{-1}. Survivin and AKT showed consistently weak binding (MM-GBSA > -30 kcal mol^{-1}) across all 26 tested compounds. The Bcl-2 gene family (Bcl-2, Bcl-W, Bcl-XL, and Mcl-1) plays a critical role in preventing cells from undergoing apoptosis. Current therapies targeting this protein family are considered a promising strategy to counteract apoptosis resistance in cancer cells.[67] Concurrently, a recent study demonstrated that targeting other anti-apoptotic proteins—including AKT, mTOR, XIAP, and survivin with Evodiamine significantly increased apoptosis rates in gastric cancer cell lines AGS and MKN45.[68] Our study identifies compounds **16**, **17**, **12**, **23**, and **24** as promising candidates due to their profoundly negative MM-GBSA values, reflecting their strong capacity to form stable complexes with and inhibit the activity of these target proteins. This molecular docking data, combined with real-time PCR and immunofluorescent analyses of several pro-apoptotic genes (as shown in Fig. 8), emphasizes that the biosynthesized Trp-AgNPs encapsulated by natural compounds from *Trevesia palmata* extract activated the apoptosis signaling pathway as a crucial mechanism leading to proliferation inhibition in gastric cancer cells.

4 Conclusion

Silver nanoparticle was successfully synthesized *via* a green synthesis approach using *Trevesia palmata* extract, resulting in small-sized nanoparticles conjugated with bioactive compounds from the herbal extract. The natural compounds present in the extract played a crucial role in reducing Ag^+ to Ag^0 and simultaneously binding to the nanoparticle surface to form the snatural compound silver nanoparticle complex Trp-AgNPs. The fabricated terpenoid-rich Trp-AgNPs exhibited anticancer efficacy against various cancer cell lines, with the highest sensitivity observed in MKN45 gastric cancer cells. The enhanced expression of Caspase 3, Caspase 8, P21, and CAV1 genes, along with the reduced expression of Bcl-2 induced by Trp-AgNPs, as well as the strong binding of several compounds on the Trp-AgNPs surface to anti-apoptotic proteins such as the Bcl-2 protein family, XIAP, and mTOR, as evaluated by molecular docking, is considered the mechanism underlying the inhibition of cell proliferation in MKN45 cancer cells. Overall, Trp-AgNPs with have shown potential as an anticancer agent. However, this study was limited to *in vitro* evaluations; therefore, testing in xenograft mouse models of gastric cancer is essential in future research to clarify their efficacy and potential for *in vivo* and eventual clinical applications.

Data availability

The data that support the findings of this study are available from the corresponding author upon reasonable request.

Author contributions

Phu Hung Nguyen, Thi Thanh Huong Le, Thi Ngoc Thuy Le, Thi Kieu Oanh Nguyen: data curation, methodology, investigation, formal analysis, writing – original draft, funding acquisition; Phu Hung Nguyen, Van Hung Hoang: conceptualization, writing – original draft, project administration, resources; Van Hung Hoang, Thi Thanh Huong Le: writing – review & editing.

Conflicts of interest

The authors declared no potential conflicts of interest with respect to the research, authorship, and/or publication of this article.

Acknowledgements

This work was financially supported by the Vietnam Ministry of Education and Training under project number: B2024-TNA-10.

References

1 R. L. Siegel, T. B. Kratzer, A. N. Giaquinto, H. Sung and A. Jemal, *Ca-Cancer J. Clin.*, 2025, **75**, 10–45.
2 T. I. Mamun, S. Younus and Md. H. Rahman, *Cancer Treat. Res. Commun.*, 2024, **41**, 100845.
3 S. Chandra, M. Gahlot, A. N. Choudhary, S. Palai, R. S. De Almeida, J. E. L. De Vasconcelos, F. A. V. Dos Santos, P. A. M. De Farias and H. D. M. Coutinho, *Food Chem. Adv.*, 2023, **2**, 100239.

4 A. Jenča, D. Mills, H. Ghasemi, E. Saberian, A. Jenča, A. M. Karimi Forood, A. Petrášová, J. Jenčová, Z. Jabbari Velisdeh, H. Zare-Zardini and M. Ebrahimifar, *Biol.: Targets Ther.*, 2024, **18**, 229–255.

5 X. Zhao and H. Qian, in *Bioactive Materials in Medicine*, Elsevier, 2011, pp. 50–69.

6 R. H. Mir, M. Maqbool, P. A. Mir, Md. S. Hussain, S. U. Din Wani, F. H. Pottoo and R. Mohi-ud-din, *Curr. Pharm. Des.*, 2024, **30**, 2445–2467.

7 I. Ijaz, A. Bukhari, E. Gilani, A. Nazir, H. Zain, R. Saeed, S. Hussain, T. Hussain, A. Bukhari, Y. Naseer and R. Aftab, *Environ. Nanotechnol. Monit. Manag.*, 2022, **18**, 100704.

8 S. D. R, A. Girigoswami, S. Meenakshi, B. Deepika, K. Harini, P. Gowtham, P. Pallavi and K. Girigoswami, *ADMET DMPK*, 2024, **12**, 177–192.

9 M. Fahim, A. Shahzaib, N. Nishat, A. Jahan, T. A. Bhat and A. Inam, *JCIS Open*, 2024, **16**, 100125.

10 G. Janani, A. Girigoswami, B. Deepika, S. Udayakumar, D. J. Mercy and K. Girigoswami, *Chem. Biodiversity*, 2025, e202500626.

11 T. A. T. Nong, T. T. H. Le, V. T. Vu, M. Q. Nguyen, D. Q. H. Can, T. H. Y. Dong, T. P. T. Nguyen, V. H. Hoang and P. H. Nguyen, *Chem. Biodiversity*, 2024, **21**, e202401065.

12 B. Lee, M. J. Lee, S. J. Yun, K. Kim, I.-H. Choi and S. Park, *Int. J. Nanomed.*, 2019, **14**, 4801–4816.

13 X. Chang, X. Wang, J. Li, M. Shang, S. Niu, W. Zhang, Y. Li, Z. Sun, J. Gan, W. Li, M. Tang and Y. Xue, *Ecotoxicol. Environ. Saf.*, 2021, **208**, 111696.

14 L. Gao, N. Wei, G. Yang, Z. Zhang, G. Liu and C. Cai, *J. Ethnobiol. Ethnomed.*, 2019, **15**, 41.

15 Y. Cao, R. Li, S. Zhou, L. Song, R. Quan and H. Hu, *J. Ethnobiol. Ethnomed.*, 2020, **16**, 66.

16 B. Kim, J. W. Han, M. Thi Ngo, Q. Le Dang, J.-C. Kim, H. Kim and G. J. Choi, *Sci. Rep.*, 2018, **8**, 14522.

17 N. De Tommasi, G. Autore, A. Bellino, A. Pinto, C. Pizza, R. Sorrentino and P. Venturella, *J. Nat. Prod.*, 2000, **63**, 308–314.

18 N. Van Hao, D. H. Tung, N. P. Hung, V. X. Hoa, N. T. Ha, N. T. Khanh Van, P. T. Tan and P. Van Trinh, *RSC Adv.*, 2023, **13**, 21838–21849.

19 N. Van Hao, D. H. Tung, N. P. Hung, V. X. Hoa, N. T. Ha, N. T. Khanh Van, P. T. Tan and P. Van Trinh, *RSC Adv.*, 2023, **13**, 21838–21849.

20 P. H. Nguyen, T. T. H. Le, D. Q. H. Can, T. N. T. Le, V. Hoang, H. P. Ngo, T. T. H. Do, T. K. O. Nguyen and V. H. Hoang, *Biocatal. Agric. Biotechnol.*, 2025, **64**, 103521.

21 C. Riccardi and I. Nicoletti, *Nat. Protoc.*, 2006, **1**, 1458–1461.

22 V. H. Hoang, T. T. H. Le, P. H. Nguyen, V. Hoang, V. K. Pham, T. K. O. Nguyen and D. Q. H. Can, *Pharmacol. Res. – Modern Chinese Med.*, 2024, **13**, 100548.

23 T. T. Huong Le, M. Q. Nguyen, V. P. Nguyen, V. H. Hoang and P. H. Nguyen, *Asian J. Plant Sci.*, 2023, **22**, 423–433.

24 T. T. Le, P. H. Nguyen, V. P. Nguyen and T. N. Nguyen, *Asian Pac. J. Trop. Biomed.*, 2023, **13**, 258–267.

25 S. N. Nangare and P. O. Patil, *Nano Biomed. Eng.*, 2020, **12**, 281–296.

26 N. Alburae, R. Alshamrani and A. E. Mohammed, *Sci. Rep.*, 2024, **14**, 4162.

27 R. Naaz, V. U. Siddiqui, S. U. Qadir and W. A. Siddiqi, *Mater. Today: Proc.*, 2021, **46**, 2352–2358.

28 S. S. Hashmi, M. Ibrahim, M. Adnan, A. Ullah, M. N. Khan, A. Kamal, M. Iqbal, A. Kaplan, N. Assad, M. S. Elshikh, S. M. Almutairi and W. Zaman, *Open Chem.*, 2024, **22**, 20240016.

29 M. Fahim, A. Shahzaib, N. Nishat, A. Jahan, T. A. Bhat and A. Inam, *JCIS Open*, 2024, **16**, 100125.

30 M. Asif, R. Yasmin, R. Asif, A. Ambreen, M. Mustafa and S. Umbreen, *Dose-Response*, 2022, **20**, 15593258221088709.

31 X. Li, B. R. Sloat, N. Yanasarn and Z. Cui, *Eur. J. Pharm. Biopharm.*, 2011, **78**, 107–116.

32 A. Dhaka, S. Chand Mali, S. Sharma and R. Trivedi, *Results Chem.*, 2023, **6**, 101108.

33 B. Mousavi, F. Tafvizi and S. Zaker Bostanabad, *Artif. Cell Nanomed. Biotechnol.*, 2025, **46**, 499–510.

34 L. Dang, J. Yang, S. Negm, A. F. El-kott, A. A. Shati, H. I. Ghamry and B. Karmakar, *Open Chem.*, 2023, **21**, 20230157.

35 S. F. Hashemi, N. Tasharrofi and M. M. Saber, *J. Mol. Struct.*, 2020, **1208**, 127889.

36 T. T. H. Le, T. H. Ngo, T. H. Nguyen, V. H. Hoang, V. H. Nguyen and P. H. Nguyen, *Biochem. Biophys. Res. Commun.*, 2023, **661**, 99–107.

37 S. Singh, H. Arya, W. Sahu, K. S. Reddy, S. Nimesh, B. S. Alotaibi, M. A. Hakami, H. H. Almasoudi, K. B. G. Hessien, M. R. Hasan, S. Rashid and T. Kumar Bhatt, *Artif. Cell Nanomed. Biotechnol.*, 2024, **52**, 238–249.

38 K. Sahu, R. Kurrey and A. K. Pillai, *RSC Adv.*, 2024, **14**, 23240–23256.

39 K. Chand, D. Cao, D. Eldin Fouad, A. Hussain Shah, A. Qadeer Dayo, K. Zhu, M. Nazim Lakhan, G. Mehdi and S. Dong, *Arab. J. Chem.*, 2020, **13**, 8248–8261.

40 M. S. Alwhibi, D. A. Soliman, M. A. Awad, A. B. Alangery, H. Al Dehaish and Y. A. Alwasel, *Green Process. Synth.*, 2021, **10**, 412–420.

41 H. Ahmed, M. Y. Zaky, M. M. A. Rashed, M. Almoiliqy, S. Al-Dalali, Z. E. Eldin, M. Bashari, A. Cheikhyoussef, S. A. Alsalamah, M. Ibrahim Alghonaim, A. M. Alhudhaibi, J. Wang and L.-P. Jiang, *Ultrason. Sonochem.*, 2024, **107**, 106923.

42 A. M. Sivalingam and A. Pandian, *Carbohydr. Polym. Technol. Appl.*, 2024, **8**, 100535.

43 A. C. Csakvari, C. Moisa, D. G. Radu, L. M. Olariu, A. I. Lupitu, A. O. Panda, G. Pop, D. Chambre, V. Socoliuc, L. Copolovici and D. M. Copolovici, *Molecules*, 2021, **26**, 4041.

44 S. Kamran, A. Sinniah, M. A. M. Abdulghani and M. A. Alshawsh, *Cancers*, 2022, **14**, 1100.

45 Hemlata, P. R. Meena, A. P. Singh and K. K. Tejavath, *ACS Omega*, 2020, **5**, 5520–5528.

46 N. S. Alduraihem, R. S. Bhat, S. A. Al-Zahrani, D. M. Elnagar, H. M. Alobaid and M. H. Daghestani, *Processes*, 2023, **11**, 301.

47 Y. Li, M. Chen, J. Li and Z. Xiong, *Inorg. Chem. Commun.*, 2024, **163**, 112277.

48 D. Huang, J. Wang, S. Zhou, T. Zhang, J. Cai and Y. Liu, *Inorg. Chem. Commun.*, 2023, **155**, 110942.

49 E. EdİZ, G. Kurtay, B. Karaca, İ. Büyük, F. Ş. GökdemİR and S. Aras, *Hacettepe J. Biol. Chem.*, 2021, **49**, 11–23.

50 H. Wu, W. Lai, Q. Wang, Q. Zhou, R. Zhang and Y. Zhao, *Front. Pharmacol.*, 2024, **15**, 1243353.

51 J. Zhang, J. Li, H. Song, Y. Xiong, D. Liu and X. Bai, *Biomed. Pharmacother.*, 2019, **109**, 806–814.

52 C. Wen, Q. Ruan, Z. Li, X. Zhou, X. Yang, P. Xu, P. D. P. Akuetteh, Z. Xu and J. Deng, *Br. J. Cancer*, 2022, **127**, 2108–2117.

53 V. Milovic, I. C. Teller, D. Faust, W. F. Caspary and J. Stein, *Eur. J. Clin. Invest.*, 2002, **32**, 29–34.

54 K.-M. Lee, J. H. Yun, D. H. Lee, Y. G. Park, K. H. Son, C. W. Nho and Y. S. Kim, *Biochem. Biophys. Res. Commun.*, 2015, **459**, 591–596.

55 S. Elmore, *Toxicol. Pathol.*, 2007, **35**, 495–516.

56 D. Huang, J. Wang, S. Zhou, T. Zhang, J. Cai and Y. Liu, *Inorg. Chem. Commun.*, 2023, **155**, 110942.

57 I. Ullah, A. T. Khalil, M. Ali, J. Iqbal, W. Ali, S. Alarifi and Z. K. Shinwari, *Oxid. Med. Cell. Longevity*, 2020, **2020**, 1–14.

58 P. E. Czabotar, G. Lessene, A. Strasser and J. M. Adams, *Nat. Rev. Mol. Cell Biol.*, 2014, **15**, 49–63.

59 M. A. Mansour, M. Rahman, A. A. Ayad, A. E. Warrington and T. C. Burns, *Cancers*, 2023, **15**, 1279.

60 X. Li, X. Li, J. Wang, Z. Ye and J.-C. Li, *Int. J. Biol. Sci.*, 2012, **8**, 901–912.

61 Z. C. Nwosu, M. P. Ebert, S. Dooley and C. Meyer, *Mol. Cancer*, 2016, **15**, 71.

62 M. I. Díaz, P. Díaz, J. C. Bennett, H. Urra, R. Ortiz, P. C. Orellana, C. Hetz and A. F. G. Quest, *Cell Death Dis.*, 2020, **11**, 648.

63 J. C. Joo, J. H. Hwang, E. Jo, Y.-R. Kim, D. J. Kim, K.-B. Lee, S. J. Park and I.-S. Jang, *Oncotarget*, 2017, **8**, 12211–12224.

64 W. Ma, D.-D. Wang, L. Li, Y.-K. Feng, H.-M. Gu, G.-M. Zhu, J.-H. Piao, Y. Yang, X. Gao and P.-X. Zhang, *Oncol. Rep.*, 2014, **32**, 293–301.

65 K. H. Nam, B. L. Lee, J. H. Park, J. Kim, N. Han, H. E. Lee, M. A. Kim, H. S. Lee and W. H. Kim, *Pathobiology*, 2013, **80**, 87–94.

66 V. Barresi, G. Giuffre', E. Vitarelli, P. Todaro and G. Tuccari, *Virchows Arch.*, 2008, **453**, 571–578.

67 A. N. Hata, J. A. Engelman and A. C. Faber, *Cancer Discovery*, 2015, **5**, 475–487.

68 J. Y. Yang, H. J. Woo, P. Lee and S.-H. Kim, *Curr. Issues Mol. Biol.*, 2022, **44**, 4339–4349.